Numerical and Experimental Investigation of Microchannel Heat Sink with Micro-Fins

Wei Long Yeo[a], Kim Ho Yeap[a], Koon Chun Lai[a], Kok Seng Ong[a] and Pei Song Chee[b]

[a]*Faculty of Engineering and Green Technology, Universiti Tunku Abdul Rahman, 31900 Kampar, Perak, Malaysia*

[b]*Lee Kong Chian Faculty of Engineering and Science, Universiti Tunku Abdul Rahman, 43000 Kajang, Selangor, Malaysia*

(Received: 17.12.2018 ; Published: 26.12.2018)

Abstract. The fluid flow and heat transfer characteristics of microchannel heat sinks with micro-fins were investigated. A comparative study was performed between the proposed heat sinks and the conventional rectangular microchannel heat sink. The result shows that the extended surface enhances the heat transfer performance. The presence of micro-fins in the heat sinks helps to disrupt the thermal boundary layer and also increases the pressure drop. The performance of the microchannel heat sink with micro-fins is found to be 16 % higher than its rectangular counterpart.

Keywords: Extended surface, Heat sink, Microchannel, Single phase flow

I. INTRODUCTION

Over the past decades, the electronic industry has witnessed the miniaturization of electronic components. Most of the electronic devices (i.e. laptop, smart phone etc.) are required to be tiny, portable and, at the same time, be able to perform tasks at a faster rate. In order to achieve this goal, high-powered integrated circuits chips have been produced. A high-powered integrated circuit chip consists of billions of transistors that operate at high frequency. Because of this reason, heat tends to be generated and trapped within the compact surface area of the chip [1]. Conventional air cooling methods appear to be insufficient to remove the excessive heat, when the heat dissipation level reaches 500 W/m^2. To solve this problem, Tuckerman and Pease have introduced the concept of microfluidic cooling technology in 1981 [2]. According to the experiment that they had conducted, a maximum of 700 W/cm^2 heat flux could be effectively removed using microfluidic cooling. Since then, microchannel heat sinks (MCHSs) have become a popular device in dissipating heat in electronic chips. The MCHS possesses high convective heat transfer coefficient, large surface area-to-volume ratio and relatively less demand of coolant inventory [3]. Over the years, the designs of the MCHSs can be mainly divided into two areas, i.e. numerical investigation [3-7] and experimental investigation [8, 9].

The conventional MCHS employs straight rectangular channel. Although the fabrication process for the conventional MCHS is relatively simple, the straight channel structure results in a very poor fluid mixing between the side wall and core flow. The regular flow in the channel leads to the gradual growth of the thermal boundary layer. Due to the progressive thickening of this layer, heat transfer effectiveness is significantly reduced [10]. In order to prevent the growth

of the thermal boundary layer in microchannel heat sinks, some of the techniques such as dimpled surface, reentrant cavities, micro-ribs etc. were introduced. These techniques enhanced the heat transfer characteristic by disturbs the thickening of the boundary layer.

In [11], Hong and Cheng have numerically studied the fluid flow and heat transfer characteristics of an offset strip-fin microchannel. They proposed different sizes of strip-fin and demonstrated how the boundary layer could be deformed to enhance the heat transfer effectiveness. They concluded that optimal results could be obtained when the fin interval to fin length (K) is equivalent to one. Mat Tokit et al. [12] proposed and analyzed an interrupted microchannel heat sink. The Nusselt number that they obtained was found to be higher than that of a conventional microchannel heat sink. As a tradeoff, however, their proposed design exhibited higher pressure drop.

Sui et al. [13] numerically studied the fluid flow and heat transfer in three-dimensional wavy MCHSs with rectangular cross sections. They reported that the wavy microchannels showed better heat transfer performance as compared to the rectangular channel with the same cross section. Mohammed et al. [14] carried out numerical simulation to study the effect of channels with different geometries on the MCHS performance. They performed a comparative study among the zigzag, curvy, step, wavy and the conventional straight MCHSs. Owing to the eddy and recirculation flows around their bend corners, the zigzag MCHS exhibited the lowest temperature and the highest heat transfer coefficient. Like [12], however, these MCHSs also produced higher pressure drop as compared to the conventional straight MCHS.

Deng et al. [15] experimentally and numerically studied the thermal enhancement in reentrant copper MCHS. They concluded that the reentrant microchannel performed better compared to the conventional rectangular straight channel due to the wider area of the heat transfer surface. The reentrant channel with an omega (i.e. Ω) shape was found to have a larger heat transfer surface as compared to its conventional counterpart. Wang et al. [16] proposed several shapes of micro-ribs and fabricated the micro-ribs using micro-electro-mechanical systems (MEMS). Their result indicated that the turbulent flow created by the micro-ribs can augment the heat transfer performance. The designs proposed by Wang et al., however, faced the same drawback as those in [12] and [14] – the pressure drop of the channels also increase and they turned out to be higher than the conventional MCHS.

As can be seen from the literature mentioned above, emphasis has been put on the optimization of the geometrical structure of the channel. Although researches such as that in [17] applied the extended surface method to enhance the performance of the MCHS, this method has not been widely and thoroughly investigated. To the best of the authors' knowledge, researches which focus on the extended surface are relatively rare in the literature. The main goal of this study is therefore to investigate the fluid flow and heat transfer characteristic numerically and experimentally by using the extended surface technique.

II. PHYSICAL MODEL

Numerical Model

In this paper, the overall dimension of the microchannel is $50 \times 3 \times 12$ mm^3. The diameter of the extended surface cylinder is set at 1 mm. A total of 11 micro-fins are constructed along the

channel and the height of each micro-fin is 5 mm. Figure 1 depicts the schematic diagram; whereas, Figure 2 and Table 1 show the geometry parameters of the microchannel heat sink.

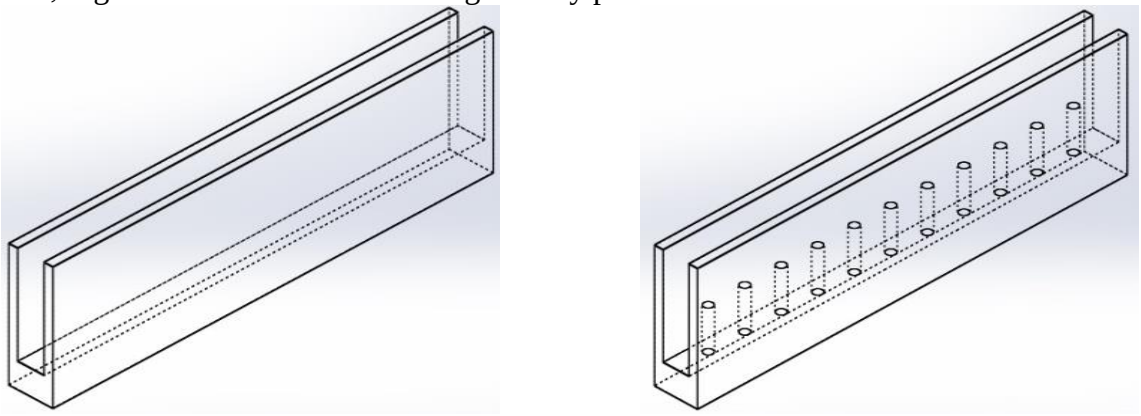

(a) (b)

FIGURE 1. Different configurations of microchannel: (a) Bare rectangular microchannel (b) Bare rectangular microchannel with micro-fins.

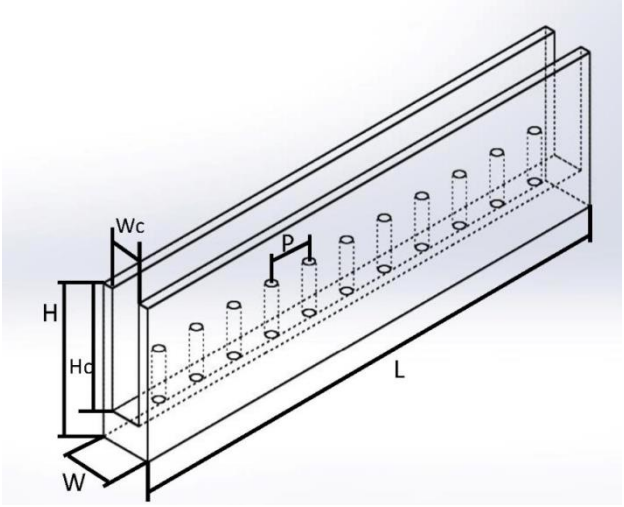

FIGURE 2. The geometry parameter of Microchannel with micro-fins.

TABLE 1. Geometric characteristics of microchannel.

Parameter	Dimension (mm)
W	5
W_c	3
H	15
H_c	12
L	50
P	4.25

In this study, a total of 12 channels were fabricated to form a microchannel heat sink. Ansys Fluent 17.2 has been employed to compute the performance of the MCHS. The SIMPLE scheme was selected to solve the pressure-velocity coupling and the third order MUSCL (Monotone

Upstream-Centered Schemes for Conservation Laws) scheme was used for discretizing the convective term in the momentum and energy conservation equations. In order to obtain a converging solution, the residual criteria used for energy equation, continuity equation, and the velocity in the *x*, *y*, *z* direction are 1×10^{-7}, 1×10^{-4} and 1×10^{-6} respectively. The following assumptions were also made in order to simplify the simulation model [17] and at the same time, to ensure that sufficiently accurate result can be obtained:

- Steady, laminar flow.
- Incompressible Newtonian fluid.
- Uniform heat flux throughout bottom wall.
- Gravitational force and radiation heat transfer are negligible.
- Conjugate heat transfer and axial wall conduction are considered.

Apart from the assumptions above, the governing equations for mass, momentum and energy are also provided and expressed as follows:

Mass conservation equation:

$$\nabla \cdot (\rho u) = 0 \tag{1}$$

Momentum equation:

$$(u \cdot \nabla)\rho u = -\nabla p + \mu \nabla^2 u \tag{2}$$

Energy equation:

$$u \cdot \nabla \mathrm{T} = \frac{\lambda}{\rho C_p} \nabla^2 T \tag{3}$$

Energy equation in the solid domain:

$$\lambda \nabla^2 T = 0 \tag{4}$$

where ρ is density of water, u represent the velocity of fluid at the inlet, p is the pressure, μ is the dynamic viscosity, λ and C_p denote the thermal conductivity and specific heat capacity of the water.

Boundary Conditions

In our study, plain water was selected as the working fluid and constant inlet velocity was applied. The ranging of the inlet velocity u was set between 0.078 to 0.23 m/s. The Reynolds number is defined as [18]:

$$Re = \rho u d / \mu \tag{5}$$

where ρ is the density of fluid, u the inlet velocity, μ the viscosity of the fluid and d is defined as the hydraulic diameter and is given in (6) below [18]:

$$d = \frac{4A}{P} = \frac{2WH}{W+H} \tag{6}$$

where A is the flow area and P represents the wetted parameter of the microchannel. The variable W and H are the width and height of the channel, respectively. The average Nusselt number is defined as [19]:

$$Nu = hd/k_{fluid} \tag{7}$$

$$h = \frac{Q}{NA_c \Delta T} \tag{8}$$

where h is the heat transfer coefficient, Q represents the total heat transfer and A_c is the water and heat sink contact surface area. ΔT can be calculated by $\Delta T = T_W - (T_{fout} - T_{fin}) / 2$, where T_W, T_{fout} and T_{fin} represent, respectively, the wall mean temperature, inlet and outlet fluid temperature.

III. EXPERIMENT SETUP

Figure 3 shows the image of the experiment setup. The corresponding apparatus and procedure are described in Figure 4. The working fluid is initially fed from the water pump to the flow sensor. The flow rate is controlled by a flow meter to assure that the volume of the working fluid is accurate. The fluid inlet and outlet were the narrowest part of the flow path and the diameter is 5 mm. The flow rate can be obtained based on the flow rate equation in (9) below:

$$Q_f = Au \tag{9}$$

where Q_f is the flow rate, A the cross-sectional of pipe and u is the velocity of fluid. When a flow rate of 4.6 ml/s is supplied into the microchannel heat sink, the fluid velocity is equal to 0.23 m/s. The Reynolds number of 0.23m/s is equivalent to 1200 and this value is known to be within the range of the laminar flow. The inlet and outlet fluid temperatures are measured by using 2 digital thermometers (DS18B20 with accuracy ±0.5 °C) – both of which are placed at the container before and after the test section.

At the test section in which the microchannel heat sink was placed, a heat source generated by an integrated LED light source (Cool RAY COB C46) is attached at the bottom of the microchannel heat sink. The integrated LED light source can provide approximately 10 W/cm^2 heat flux through the bottom wall of microchannel heat sink. Figure 5 shows the fabricated microchannel heat sink. In the experiment, the top surface of microchannel is covered by a layer of transparent perspex so as to enclose the passage for fluid flow and to allow better observation of fluid flow. An infrared IR camera (Fluke Tis55 Thermal Imager) and four K type thermocouples are used to measure the wall temperature of the microchannel heat sink. The locations of the 4 thermocouples are 20 mm, 30 mm, 40 mm, and 50 mm respectively from the inlet and 1.5 mm above the bottom surface. Figure 6 shows the side view of the microchannel heat sink.

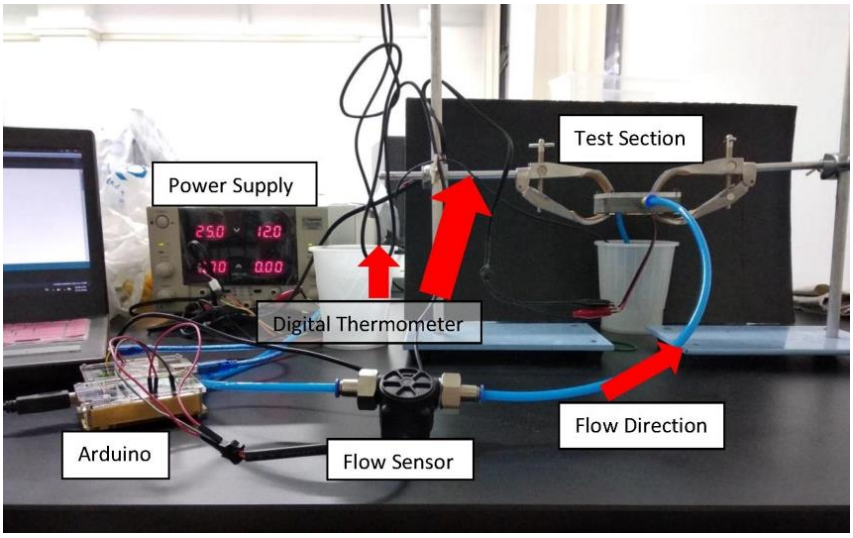

FIGURE 3. Image of the experimental setup.

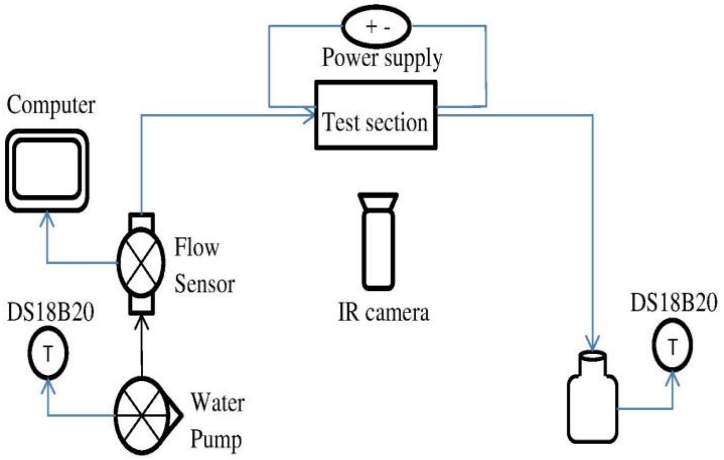

FIGURE 4. Schematic diagram of the experimental setup.

(a) (b)

FIGURE 5. Fabricated MCHS (a) Bare rectangular microchannel (b) rectangular microchannel with micro-fin.

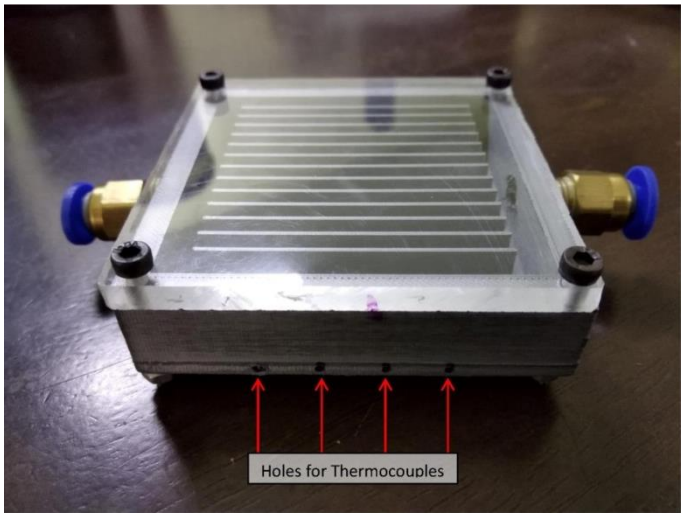

FIGURE 6. Side view of Bare rectangular microchannel heat sink.

IV. RESULTS AND DISCUSSION

Flow Distribution

Figure 7 illustrates the fluid flow velocity distribution of the microchannel heat sink at *z*-plane = 25mm and *Re* = 1200. As shown in Figure 7(a), the fluid flow reaches its maximum velocity at the centre of the microchannel. This phenomenon causes the continuous thickening of thermal boundary layer. Inefficient fluid mixing between the side wall and the middle portion results in the poor heat transfer performance. The presence of the micro-fins at the centre portion of the microchannel acts as a disrupter. As can be observed in Figure 7(b), the micro-fins induce recirculation flow and they help to disrupt the thermal boundary layer.

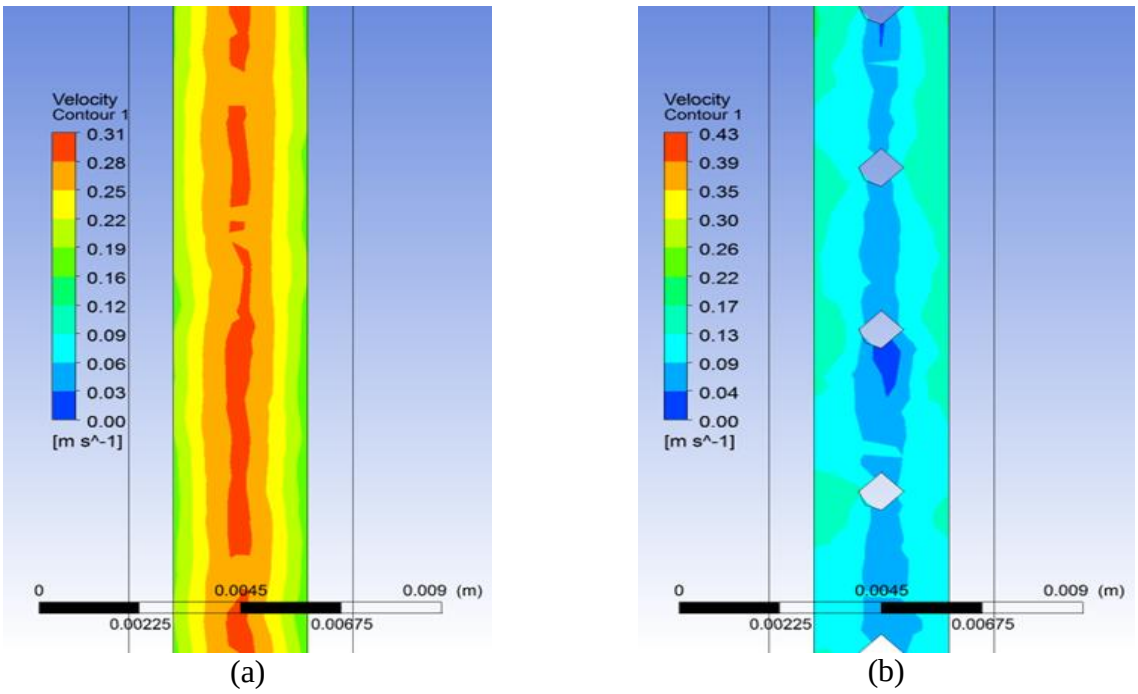

FIGURE 7. Velocity distribution flow from top to bottom (a) Bare rectangular microchannel (b) rectangular microchannel with micro-fins.

Temperature Distribution

Figure 8 displays the temperature distribution of the microchannel heat sink at *z*-plane = 25mm and *Re* = 1200. As shown in Figure 8, the microchannel with micro-fins has lower wall temperature compared to the conventional rectangular microchannel. This shows that the micro-fins play an important role in augmenting the heat transfer characteristics. Figure 9 depicts the variation of Nusselt number with Reynolds number. Tables 2 and 3 tabulate the experiment and simulation results of the wall temperature and Nusselt number. Upon close inspection on both tables, it can be seen that the simulation and experiment results agree reasonably well. The maximum discrepancies for the bare rectangular microchannel and the bare rectangular with micro-fins are 8.33 % and 7.15 % respectively. We attribute the discrepancy to the adiabatic environment assumed in the simulation. In the actual experiment, the top surface of the microchannel is covered by a layer of Perspex which may result in heat loss. This phenomenon is similar to that observed in [15].

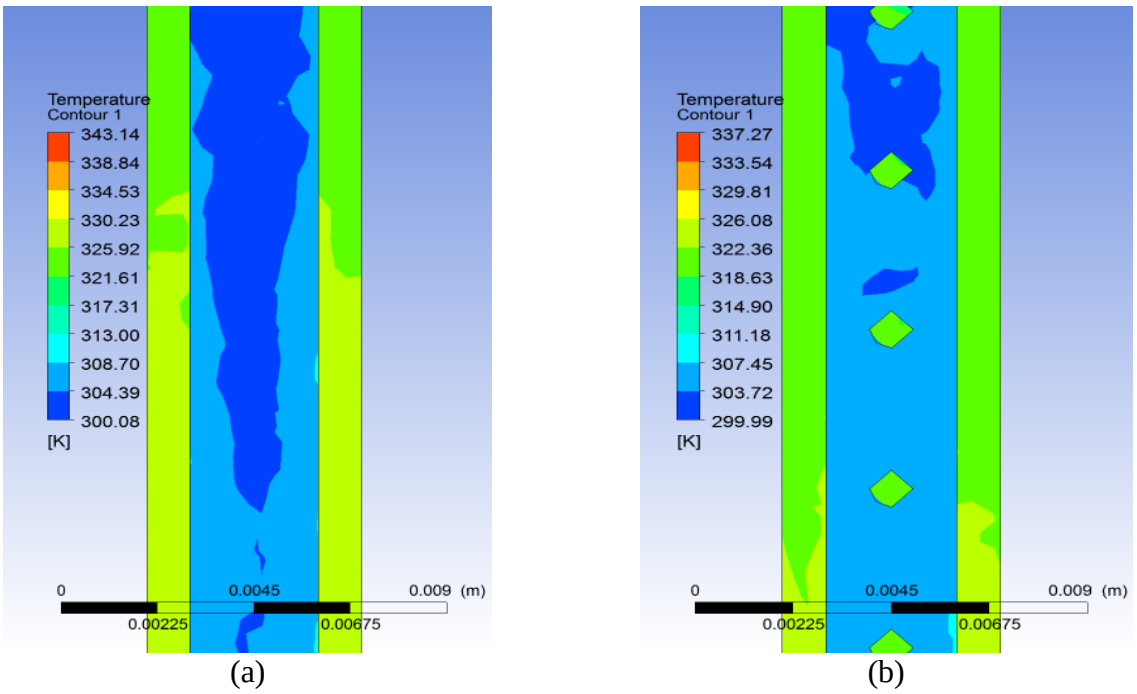

FIGURE 8. Temperature distribution flow from top to bottom (a) Bare rectangular microchannel (b) rectangular microchannel with micro-fins.

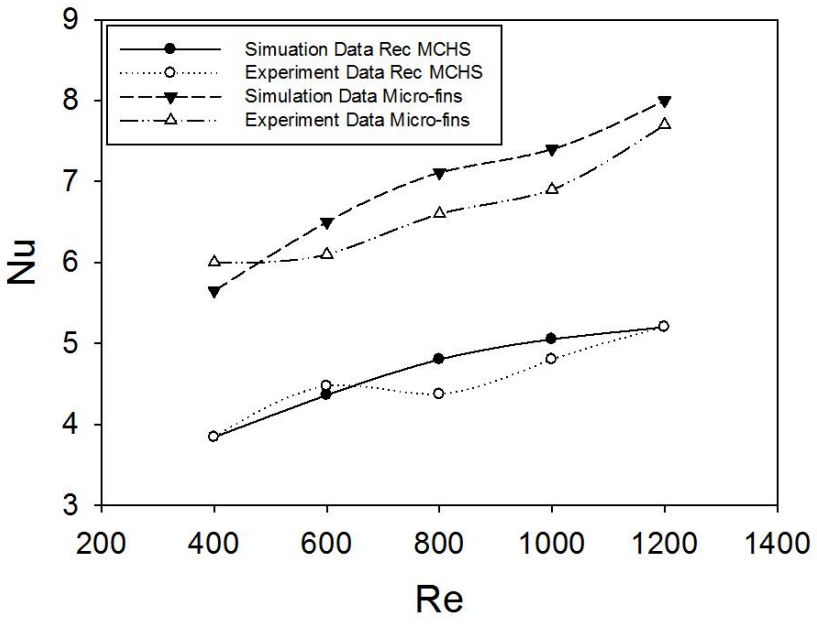

FIGURE 9. Variation of Nusselt number with Reynolds number.

TABLE 2. The experiment and simulation results of bare rectangular microchannel

Reynolds Number (RE)	T_w (Simulation)	T_w (Experiment)	Nusselt Number (Simulation)	Nusselt Number (Experiment)	Discrepancy (%)
400	353.0	347.1	3.84	3.83	0.26
600	348.0	343.7	4.36	4.47	2.52
800	346.0	341.8	4.80	4.40	8.33
1000	344.0	340.0	5.05	4.80	4.95
1200	343.0	339.0	5.20	5.19	0.19

TABLE 3. The experiment and simulation results of bare rectangular microchannel with micro-fins

Reynolds Number (RE)	T_w (Simulation)	T_w (Experiment)	Nusselt Number (Simulation)	Nusselt Number (Experiment)	Discrepancy (%)
400	347.0	340.0	5.65	6.00	6.20
600	342.0	337.0	6.50	6.10	6.15
800	340.0	335.0	7.11	6.60	7.17
1000	338.0	334.0	7.40	6.90	6.75
1200	337.0	333.7	8.00	7.70	3.75

Pressure drop characteristics and thermal performance

Figure 10 illustrates the variation of pressure drop with Reynolds number. The increase of the pressure drop is in direct proportion with the Reynolds number. The results are in agreement with those in [20, 21]. The presence of the micro-fins reduces the area of fluid flow. Hence, we ascribe the increase of the pressure drop to the sudden contraction of the flow area which slows down the fluid flow. When the fluid impinges the micro-fins, the central flow is separated from the transverse fluid flow and the recirculation zone. This helps to mix the fluid located at the side wall region with that at the central core flow. This phenomenon also contributes to the increase of the pressure drop. The thermal performance of this study can be calculated from (10) below [22]:

$$\eta = \frac{Nu / Nu_0}{\left(\Delta P / \Delta P_0\right)^{1/3}} \tag{10}$$

In comparison with the conventional rectangular microchannel, the thermal performances of microchannel heat sinks with micro-fins are 16.8%, 16%, 12.3%, 9.1% and 12.6% higher at Reynolds number *Re* = 400, 600, 800, 1000 and 1200, respectively. It shows a decreasing trend when the Reynolds number increases. We attribute this to the increase of the pressure drop when Reynolds number increases.

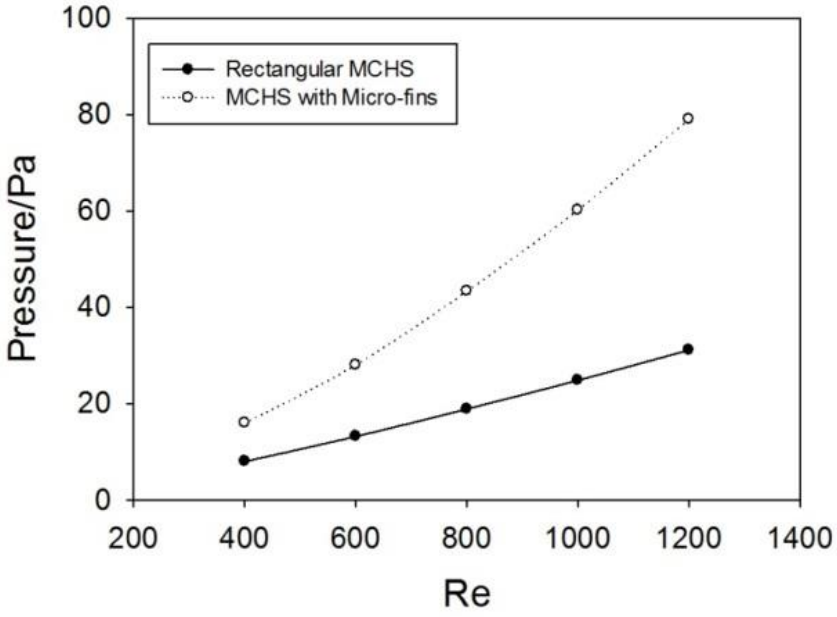

FIGURE 10. Variation of Pressure drop with Reynolds number

V. CONCLUSION

In this study, microchannel heat sinks with micro-fins were developed and validated. The fluid flow and heat transfer characteristics were investigated. The results show that the microchannel with micro-fins has better heat transfer performance than the conventional rectangular microchannel. The maximum performance of the microchannel with micro-fins is found to be 16.8% higher than the rectangular microchannel.

ACKNOWLEDGMENTS

The project is funded by the University Internal Fund (UTARRF) under project IPSR/RMC/UTARRF/2016-C1/L1.

REFERENCES

1. B. Agostini, M. Fabbri, J.E. Park, L. Wojtan, J.R. Thome, and B. Michel, *Heat Transfer Engineering* **28**, 258 (2007).
2. D. Tuckerman and R. Pease, *IEEE Electron Device Letters* **2**, (1981).
3. M. Hatami and D. Ganji, *Energy Conversion And Management* **78**, (2014).
4. M. Rahimi-Gorji, O. Pourmehran, M. Hatami and D. Ganji, *The European Physical Journal Plus* **130**, (2015).
5. G. Xie, S. Li, B. Sunden and W. Zhang, *International Journal Of Numerical Methods For Heat & Fluid Flow* **24**, (2014).
6. C. Leng, X. Wang, W. Yan and T. Wang, *Energy Conversion And Management* **110**, (2016).
7. L. Chai, G. Xia and H. Wang, *Applied Thermal Engineering* **92**, (2016).

8. F. do Nascimento, H. Leão and G. Ribatski, *Experimental Thermal And Fluid Science* **45**, (2013).
9. P. Lee, S. Garimella and D. Liu, *International Journal Of Heat And Mass Transfer* **48**, (2005).
10. L. Lin, J. Zhao, G. Lu, X. Wang and W. Yan, *International Journal Of Thermal Sciences* **118**, (2017).
11. F. Hong and P. Cheng, *International Communications In Heat And Mass Transfer* **36**, (2009).
12. E. Tokit, H. Mohammed and M. Yusoff, *International Communications In Heat And Mass Transfer* **39**, (2012).
13. Y. Sui, C. Teo, P. Lee, Y. Chew and C. Shu, *International Journal Of Heat And Mass Transfer* **53**, (2010).
14. H. Mohammed, P. Gunnasegaran and N. Shuaib, *International Communications In Heat And Mass Transfer* **38**, (2011).
15. D. Deng, W. Wan, Y. Tang, H. Shao and Y. Huang, *International Journal Of Heat And Mass Transfer* **91**, (2015).
16. G. Wang, D. Yang, Y. Wang, D. Niu, X. Zhao and G. Ding, *Sensors* **15**, (2015).
17. V. Yadav, K. Baghel, R. Kumar, and S. Kadam, *International Journal of Heat and Mass Transfer* **93**, 612 (2016).
18. Y. Li, G. Xia, D. Ma, Y. Jia, and J. Wang, *International Journal of Heat and Mass Transfer* **98**, 17 (2016).
19. Y. Jia, G. Xia, Y. Li, D. Ma and B. Cai, *International Communications In Heat And Mass Transfer* **92**, (2018).
20. C. Zhang, Y. Chen and M. Shi, *Chemical Engineering And Processing: Process Intensification* **49**, (2010).
21. W. L. Yeo, K. H. Yeap, K. C. Lai, K. S. Ong, P. S. Chee, *Applications of Modelling and Simulation* (AMS) **2**, 102 (2018).
22. Y. Li, F. Zhang, B. Sunden, and G. Xie, *Applied Thermal Engineering* **73**, 185 (2014).